https://doi.org/10.18321/ectj1029

Porous Nickel Based Half-Cell Solid Oxide Fuel Cell and Thin-Film Yttria-Stabilized Zirconia Electrolyte

A.G. Umirzakov[1,2]*, A.L. Mereke[1,2], A.A. Shaikenova[1,2], B.A. Rakhmetov[2], M.A. Yeleuov[1], R.E. Beisenov[1,2], R. Ebrahim[3], B.A. Mansurov[4]

[1]Satbayev University, 22 Satbaev str., Almaty, Kazakhstan
[2]Institute of Physics and Technology, 11 Ibragimova str., Almaty, Kazakhstan
[3]University of Houston, Houston, TX 77204-5004, USA
[4] Abai Kazakh National Pedagogical University, 13 Dostyk ave., Almaty, Kazakhstan

Article info

Received:
17 August 2020

Received in revised form:
8 October 2020

Accepted:
16 December 2020

Keywords:
Thin-film solid oxide fuel cells,
Porous anode,
Pore-forming agent,
Electrolyte,
Pulsed laser deposition.

Abstract

In this work, a porous nickel anode for thin-film solid oxide fuel cell prepared by the simple powder hot-pressing method is investigated. Powders of Ni and pore-forming agent (PFA) were thoroughly mixed in different ratios, pressed in a mold and further sintered. The polishing technique with Yttria-Stabilized Zirconia (YSZ) powder has been developed to decrease the surface roughness of Ni-based anode in order to deposit a crack-free electrolyte layer. The 3 μm YSZ thin-film electrolyte was deposited by the pulsed laser deposition technique on the surface of the anode. Morphological and elemental analyses of the samples were characterized by scanning electron microscopy (SEM) and energy dispersive spectroscopy (EDS) analyses. X-ray diffraction was used for phase analysis and structural characterization. The specific surface areas of the resulting anodes were calculated from their isotherms of N_2 adsorption and desorption using the Sorbtometer and calculated by Brunauer Emmett-Teller (BET) method. As a result, the highest mechanical strength and specific surface area (15.42 m^2g^{-1}) possessed a sample with the content of PFA equal to 40%, while its ionic conductivity at 800 °C reached $6.4 \cdot 10^{-2}$ S/cm.

1. Introduction

Currently, the rapid pace of world economic development has a negative impact on the environment due to the fact that fossil fuels are the main source of energy in the world [1], and it is estimated as 80% [2]. The lack of traditional fossil fuels, their low efficiency and environmental potential have led to the active development, study and application of alternative energy sources [2–4]. This trend is crucial in the development of new highly efficient energy systems and the creation of an environmentally friendly society. Recently, fuel cells (FC) have been actively investigated as an effective source of environmentally friendly energy [5].

Solid oxide fuel cells (SOFCs) in near future have the excellent opportunity to be one of the "greenest" and highly efficient energy technologies in the field of direct conversion of chemical fuels to electricity [6–8]. Today, economically competitive SOFC systems already exist, apparently ready for commercialization, but the widespread penetration of the technology into the market requires constant innovation of materials and manufacturing processes to increase the system service life and reduce the costs [9].

Among the numerous types of FC, such as alkaline FC [10, 11], FCs with proton-exchange membrane [12–14], FCs based on carbon compounds [15, 16], solid oxide fuel cells (SOFCs) based on oxygen-conducting solid electrolytes, which have a high efficiency (up to 60%) and can use not only pure hydrogen but also various hydrocarbons as a fuel, should be highlighted. The main structural components of these SOFCs are porous electrodes (anode and cathode) and a solid gas-tight electrolyte (ZrO_2: Y_2O_3 (YSZ)) located between them [1].

*Corresponding author.
E-mail: arman_umirzakov@mail.ru

The main advantage of the SOFCs over other FCs is that they are characterized by high efficiency and possess the ability to convert chemical fuel directly into electrical and thermal energy without the use of expensive catalysts [16]. Various types of fuel, such as hydrogen or natural gases, can be used in the operation of the SOFCs [17]. The mechanism of SOFCs operating is the following: at the anode part, hydrogen is oxidized, and the released electrons are removed to the external circuit [18]. Air is supplied to the cathode part, and oxygen is reduced to O^{2-} by reacting with electrons from the external circuit. The oxygen ions pass through gas-tight and an ion-conducting electrolyte between the anode and cathode under the condition of heating the electrolyte to ~ 900 °C, depending on the nature of the electrolyte material [19]. Subsequently, on the anode part, the oxygen ions combine with the H_2 to form water vapor. Water and CO_2 are the main reaction products on the anode part. The known most effective material for the creation of anodes is the so-called "cermet", which is a composite based on Ni (or NiO) and YSZ [9, 8–20].

When manufacturing SOFCs, the anode layer must meet some conditions:

1) the contact between nickel particles must be good enough, otherwise, the electrochemical reaction will be limited only by the surface and the current will flow only along the ion paths through the porous YSZ layer, which will cause large ohmic losses;

2) the tight contact between YSZ particles is a important factor because the thickness of the layer in which the electrochemically active sites are distributed is determined by the ratio of the ohmic resistance of ion transfer and polarization resistance at the Ni-YSZ contact;

3) the close contact between nickel and YSZ is required for the long-term stability of the material since if there is empty space around the nickel particles, they will start to sinter.

To avoid this, the space between them must be evenly filled with YSZ. However, a certain number of pores should still remain to facilitate the transport of reacting and formed gases, since low values of the gas diffusion coefficients affect the performance of the entire element [9].

The way to reduce the operating temperature of the SOFCs is to fabricate electrolytes with a layer size less than 10 μm. This approach will reduce the internal resistance and increase the power of the element. In our research, the step of reducing the size of electrolytes is the main solution for lowering the operating temperature of SOFCs. However, in traditional SOFC systems, a significant reduction of the electrolyte layer can critically affect the fuel cell due to the strength characteristics, since the electrolyte acts as a supporting element of the entire cell [21, 22]. In this regard, the current study is focused on the fabrication of half-cell SOFC with the highly porous structure of Ni anode with yttria stabilized zirconia (YSZ) particles between the anode and electrolyte layer deposited by pulsed laser deposition technique (PLD).

2. Experimental

2.1. Fabrication of macroporous nickel

Macroporous Ni was obtained by mixing of nanoscale Ni powder (Alfa Aesar, 99.999%, 70–100 nm) with a pore-forming agent (PFA, ammonium compound) in various ratios (95:5, 90:10, 80:20, 70:30, 60:40), followed by pressing, evaporation, and annealing of the resulting mixture. The mixture was placed in a steel mold and pressed under the 500 kg/cm^2 pressure. The resulting sample of a round shape with a diameter of 2 cm was then heated for 2 h at 80 °C for uniform evaporation of PFA. Further, the sample was sintered and reduced in a furnace at 900 °C in the atmosphere of hydrogen to density Ni particles and eliminate from PFA completely.

2.2. Polishing the surface of macroporous nickel with Ni-YSZ powder

The surface of the porous nickel was polished at a mechanical polishing machine. The Ni-YSZ powder with the ratio 3:1, mixed with a glycerin binder, was used as a polishing agent. The resulting paste was deposited on the surface of the porous Ni sample, the sample was polished for 15–30 min and annealed up to 900 °C in the atmosphere of hydrogen again. This process helps to clog macropores of Ni with YSZ to provide a transit layer between anode and electrolyte.

2.3. Deposition of a thin layer of YSZ electrolyte on polished Ni-YSZ by PLD

Thin layer deposition was performed on the PLD equipment with the KrF excimer laser (Lambda Physik, LPX210 model) with a wavelength of 248 nm. The electrolyte and cathode layers were deposited on the porous surface of a nickel anode under a frequency of 7 Hz and energy of 380 mJ.

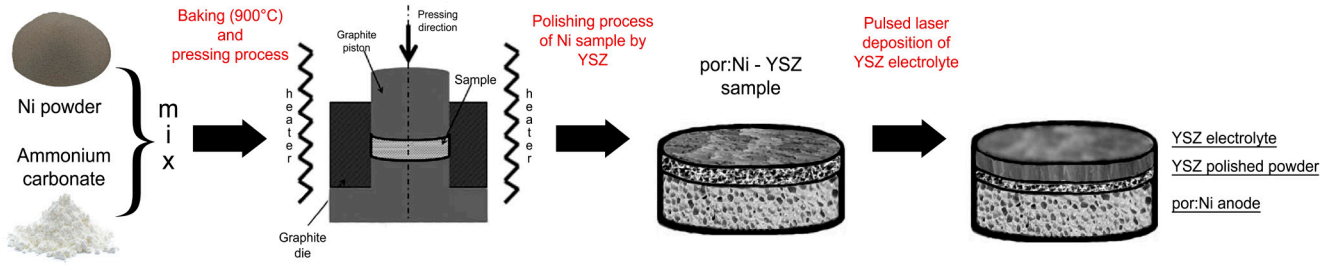

Fig. 1. Schematic illustration of half-cell SOFC fabrication process.

The stainless steel chamber was evacuated down to 10^{-6} Pa pressure with the use of a turbomolecular pump. The substrate surface was heated up to 600 °C by the holder resistive heater, the target was located at a distance of 6 cm under the substrate holder. Before deposition, to prevent droplet ejection and to remove surface impurities, the laser beam irradiated the target [23]. The dense layer of YSZ electrolyte with a thickness of about 3 μm was deposited on the Ni-YSZ at 650 °C in the mixed atmosphere of argon and hydrogen (96:4%) to prevent nickel oxidation. Figure 1 presents a schematic illustration of a half-cell SOFC fabrication process.

2.4. Sample impedance measurement technique

The impedance was measured in single chamber equipment made entirely of fused silica. The platinum paste was applied to the electrolyte serving as electrode contacts (Fig. 2). The cell was uniformly heated in a tubular furnace, and the impedance spectra were recorded in the frequency range from 0.1 Hz up to 100 kHz. The amplitude RMS (the root mean square) value of the alternating current was 20 mV, the temperature range of 500–800 °C [24]. The gas supply was about 30 sccm, while the pressure in the chamber was controlled by continuous pumping of the chamber. Before the measurements, the sample was heated at 800 °C for 6 h to eliminate the possible contaminants [24–26].

2.5. Sample characterization

YSZ (111, 200, 220, 311) film and porous Ni anode (111, 220) were characterized using several techniques. The deposited films surface morphology was studied by scanning electron microscopy and atomic force microscopy (SEM and AFM). The thickness of the cell and interface of the films was studied by cross-section SEM. The orientation and crystallinity of the deposited layers were

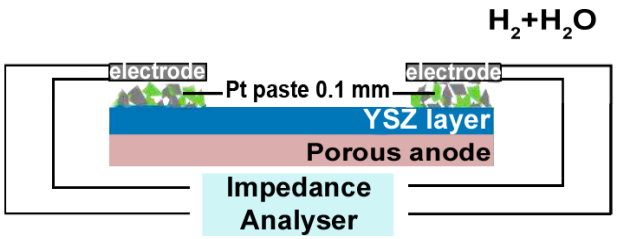

Fig. 2. Scheme of electrolyte layer impedance measurements.

determined by X-ray diffraction (XRD). The specific surface areas of the resulting anodes were calculated from their isotherms of N_2 adsorption and desorption using the Sorbtometer and calculated by Brunauer Emmett-Teller (BET) method.

3. Results and discussion

The SEM and EDS analysis of Ni powder are presented in Fig. 3a and b. From SEM images, the powder has a particle size of about 100 nm with good homogeneity. Powder grains' size is an essential factor in obtaining anode with a homogeneous and extensive porous structure [27]. The high porosity of the anode is the main requirement for the unhindered delivery of hydrogen to the anode/electrolyte reaction zone. The results of EDS analysis confirm the presence of Ni with no impurities.

The furnace annealing profile stages are presented in Fig. 4a. It was experimentally found that it is important to heat the anode as slowly as possible; this is due to the process of pore formation in the nickel structure. Sharp temperature jumps provoke active evaporation of the PFA, which forms macropores, causing surface cracking and destruction of the entire sample [28]. Thus, a slow pore-former evaporation rate (120 min) was chosen and the sample was cooled for 6 h. Figure 4b demonstrates the treated and polished porous nickel anode samples with dimensions 10×10 mm.

(a)

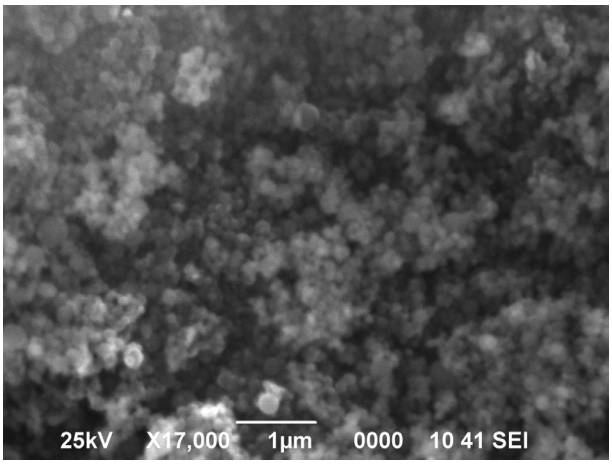

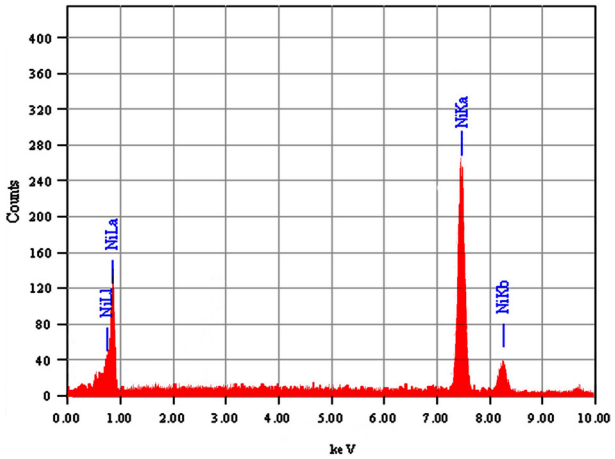

(b)

Fig. 3. SEM image (a) and EDS analysis (b) of Ni powder.

(a)

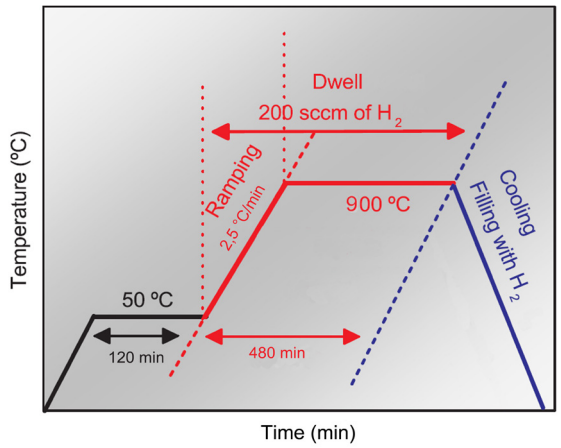

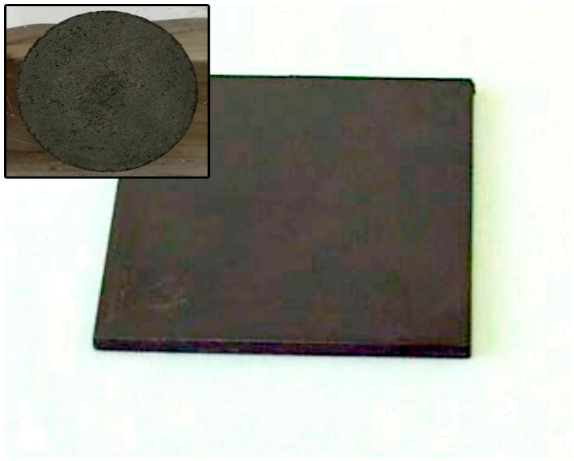

(b)

Fig. 4. The temperature profile (a) for the annealing process and the porous nickel anode after polishing (b) 10×10 mm.

(a)

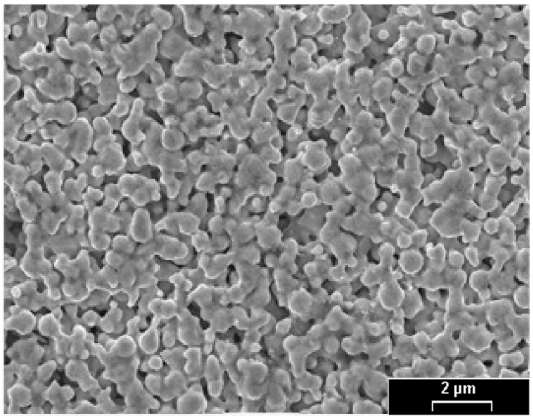

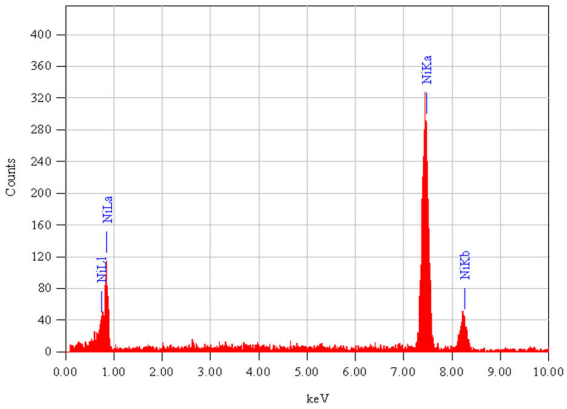

(b)

Fig. 5. The surface morphology of Ni porous anode (a) and EDS analyses (b) of polished porous nickel anode with dimension 10×10 mm.

The SEM surface analysis showed that the nickel particles were well sintered together forming a porous homogeneous structure (Fig. 5a). The EDS was conducted to verify the purity of the porous Ni sample composition after annealing. The SEM image and EDS analysis are presented in Fig. 5a and b, demonstrate that the sintered anode contains about 99 wt.% of Ni, which confirms the complete evaporation of PFA during annealing.

After the sintering of anodes, their surface morphology was studied by SEM (Fig. 6a–e). From the images, the surface of Ni-based anode is presented by porous structure with diameter of pores in the range from 200 nm up to 1 µm. It can be seen that

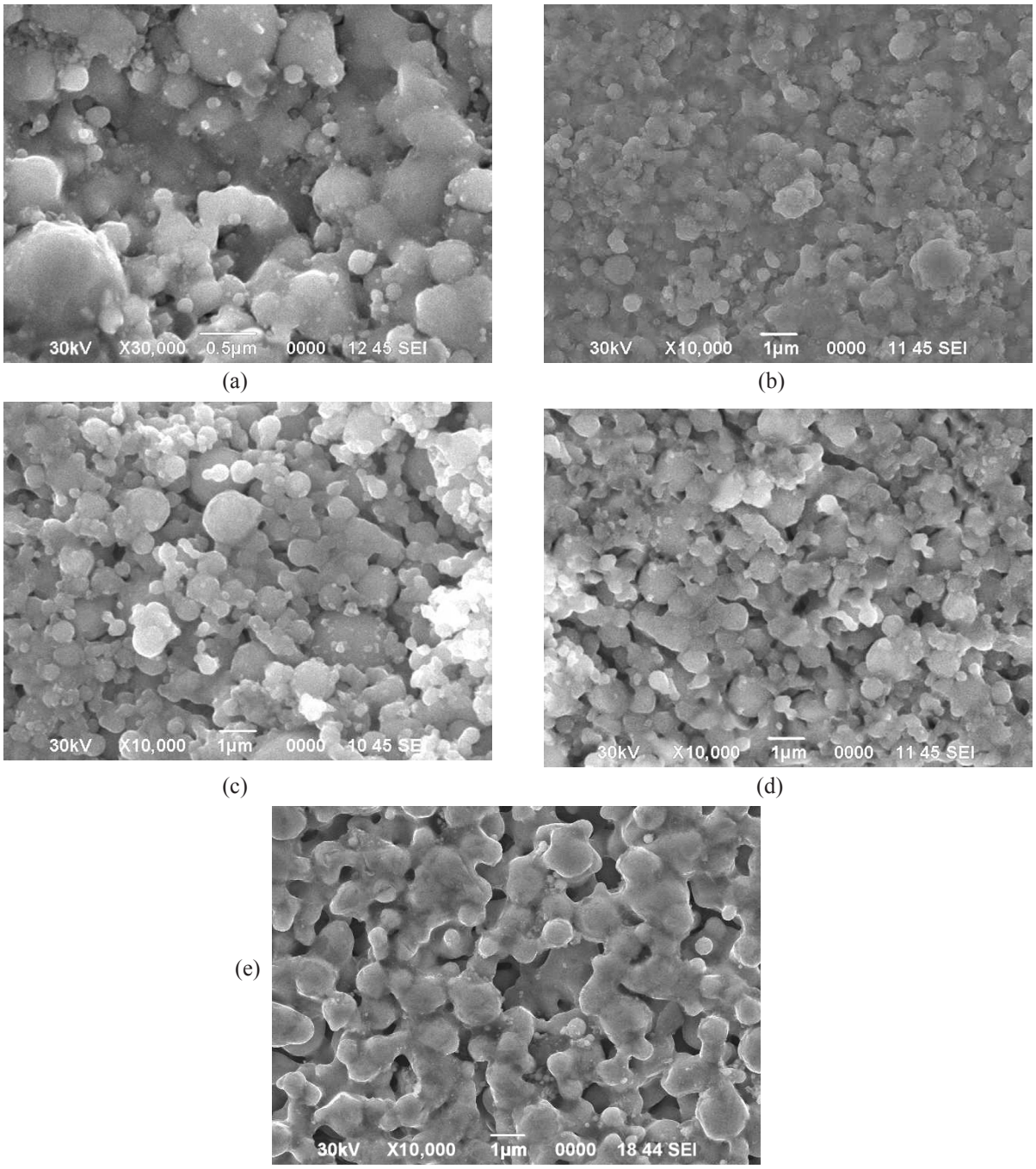

Fig. 6. SEM images of the porous nickel anodes with different Ni: PFA ratios: (a) – 95:5%; (b) – 90:10%; (c) – 80:20%; (d) – 70:30%; (e) – 60:40% .

nickel powder particles were sintered together after they reached the melting phase, which improves the mechanical properties of the whole anode. With an increase in the amount added to the mixture PFA, the number and quality of pore-channels observed in the images increases [29].

Gas adsorption was performed using Sorbtometer equipment. Adsorption was conducted using N_2 gas (99.999%). It was experimentally found that the highest value of specific surface area (15.42 m^2g^{-1}) exhibited the sample with 40% of PFA (Fig. 7). From the graph, it can be seen that specific surface area is growing in the range of PFA addition starting from 5 up to 40%, at which it reached the highest value. Further increase in PFA content in the system led to upsize of pore diameter and decrease mechanical strength of the samples [30].

PLD deposition of YSZ electrolyte was carried out on an untreated sample of a porous Ni-based anode, the surface morphology of which is presented in Fig. 8a. The deposited layer uniformly coated the surface of the anode, repeating its structure granularity. Non-electrolyte-coated pores were found on the surface (Fig. 8b), which is unacceptable in

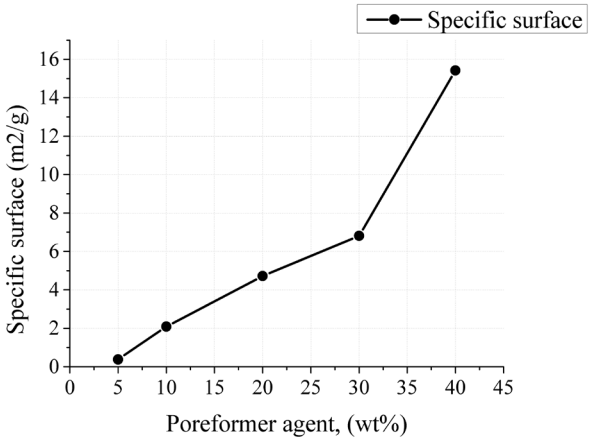

Fig. 7. Graph of dependence of the specific surface on PFA.

fuel cells due to possible hydrogen leakage. In this regard, it was decided to conduct the surface treatment of the anode by polishing and smoothing its surface to deposit the uniform layer of electrolyte.

The mechanical treatment process of the anode surface was carried out for the formation of a solid and flat surface. The pore diameters of Ni-based anode are less than 500 nm, so that the thin electrolyte layer can be deposited as a solid sealed layer, which is beneficial for avoiding the passage of gases from the anode and cathode parts. The polishing was carried out by using a mixture of Ni and YSZ powders, which make it possible to form a smooth surface at the anode/electrolyte interface and increase a triple-phase boundary area.

Figure 9 presents SEM image of the surface morphology of the polished Ni-based anode. It can be seen that the surface of Ni anode became smoother, its diameter of pores slightly decreased compared to the surface of Ni-based anode without polishing (Fig. 6). Thus, the formation of the smooth surface structure after polishing is beneficial for avoiding the degradation of the fuel cell due to the coefficient of thermal expansion of the cermet structure during the operation of SOFCs. As a result, the smooth anode surface allowed depositing a homogeneous layer of YSZ electrolyte with a thickness of ~ 3 μm, which effectively prevents the traveling of hydrogen to the cathode part of the SOFC.

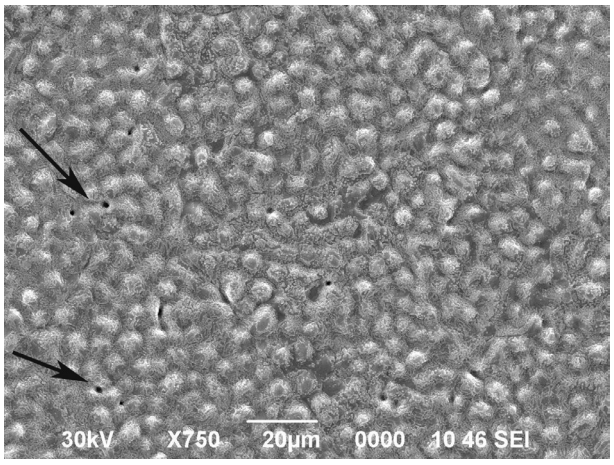

(a)

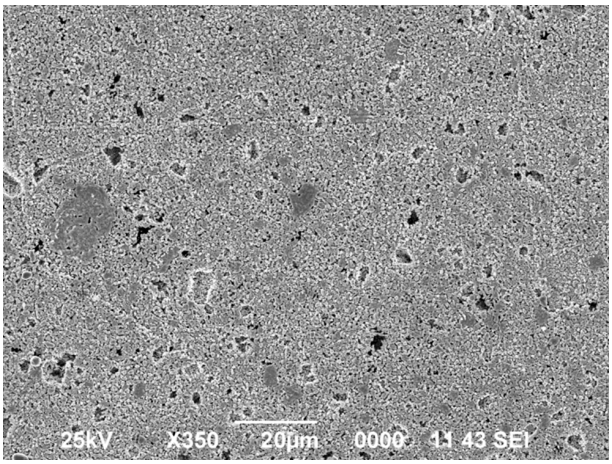

(b)

Fig. 8. SEM images of surface morphology of Ni-based anode before PLD (a) and after deposition of a thin YSZ electrolyte layer (b).

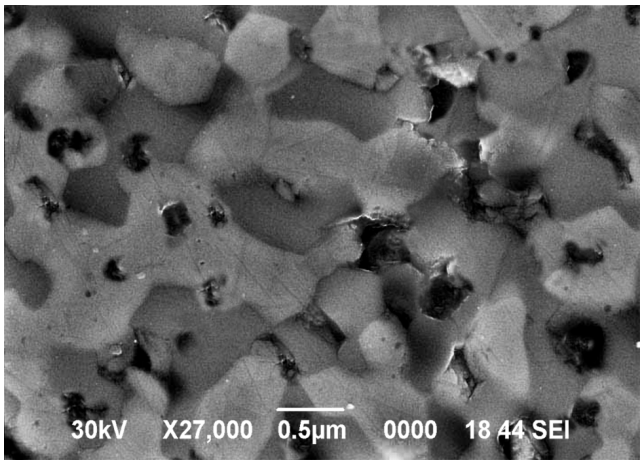

Fig. 9. SEM morphology of Ni-based anode after polishing with YSZ powder.

The cross-section and surface morphology of the resulting Ni/YSZ based SOFC was characterized by SEM (Figs. 10a and b). From Fig. 10a it is seen that the deposited YSZ electrolyte layer has a thickness of ~ 3 μm with no cracks in the structure. However, the surface of YSZ electrolyte is not uniform, in some areas it repeats the surface of the porous nickel. Long duration of PLD results in the complete coating of porous Ni surface with electrolyte and filling the pores, thus increasing the triple-phase boundary of the SOFC.

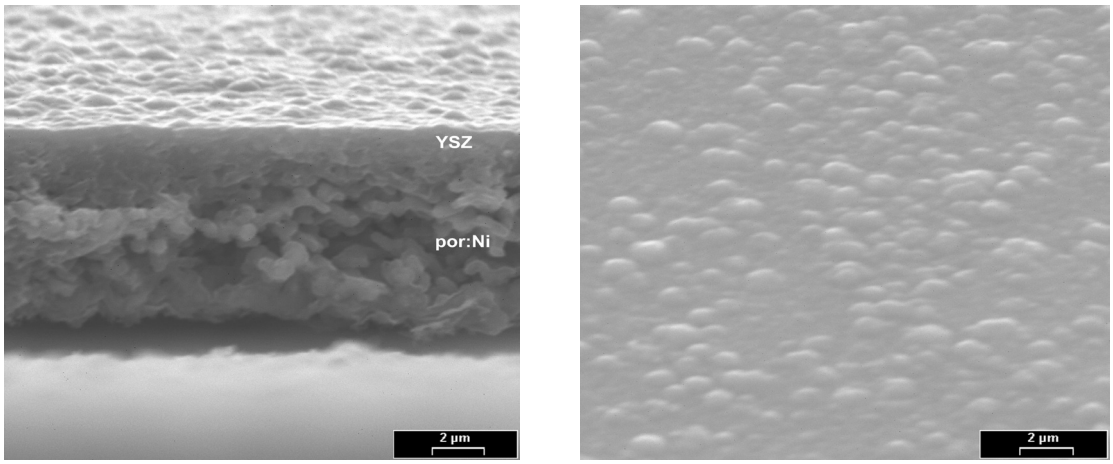

Fig. 10. SEM images of cross-section of obtained porous Ni-based anode with YSZ electrolyte layer (a) and its surface morphology (b).

Figure 11 demonstrates the X-ray diffraction patterns of the porous anode (black line) and resulting SOFC based on NI/YSZ, obtained by PLD (red line). The X'Pert HighScore with the database PDF-2 2013 was used for processing the X-ray diffraction patterns data. From the spectra it can be seen that the reflections occur at 2θ equal to 45.8°, 53°, 77.3° which corresponds to the Ni orientation planes (111), (200), (220) (black line). The red line in Fig. 11 presents the reflections at 2θ equal to 30, 35, 46, 50, 53, 59 and 77 corresponding to YSZ (111), YSZ (200), Ni (111), YSZ (220), Ni (200), YSZ (311) and Ni (220), respectively. Based on the results of XRD it can be concluded that after annealing of the sample, no extraneous elements were found in its structure, the process was chemically pure.

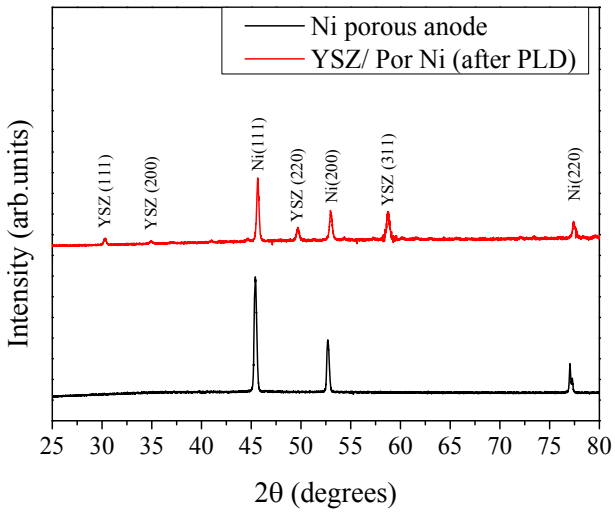

Fig. 11. XRD of the obtained SOFCs based on porous Ni anode coated with YSZ electrolyte (red line) and porous free-electrolyte Ni (black line).

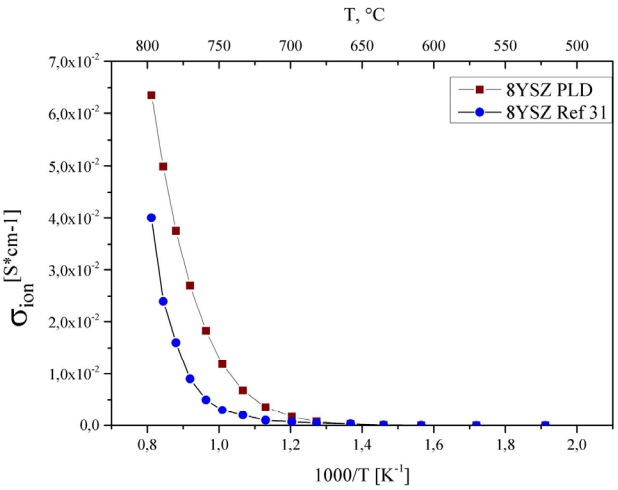

Fig. 12. Ionic conductivity of the YSZ phase.

Figure 12 presents the dependence of the ion conductivity of half-cell SOFC based on porous Ni/YSZ against 1000/T. The value of activation energy in the temperature range from 700 up to 800 °C is equal to 0.42 eV. It was experimentally found that the ionic conductivity of YSZ phase is $6.4 \cdot 10^{-2}$ S/cm at 800 °C, while the value of ionic conductivity of YSZ described in [31] is lower, it reached approximately 4×10^{-2} S/cm for 8 mol.% YSZ. This can be explained by the low thickness of YSZ electrolyte layer (~ 3 μm) deposited by PLD technique.

4. Conclusion

In summary, the possibility of forming SOFCs anode using nickel nanopowder and PFA in various ratios has been studied. Based on the results of SEM and measurements of the specific surface

area, it can be noted that the most developed porous structure in a pair with good sinterability of nickel nanoparticles was possessed by a sample with Ni to PFA ratio as 60:40%. The EDS analysis confirms the purity of experiments and the absence of elemental impurities in the resulting materials. The purposed technique of polishing macroporous Ni-based anode by Ni-YSZ powder allows depositing uniform and defect-free thin YSZ electrolyte layer by PLD, which decreases thermal expansion difference, and increases the triple-phase boundary of the fuel cell, whereas anode polishing reduces the pore size at the junction with the electrolyte. The measured ionic conductivity of ~ 3 μm thin-film electrolyte reached $6.4 \cdot 10^{-2}$ S/cm at 800 °C, which is several orders of magnitude higher compared to the existing analogs. This can be explained by the fact that with the decrease of electrolyte film thickness, its total conductivity increases by about an order of magnitude. At the same time, an increase in the content of zirconium dioxide leads to a decrease in the contribution of the bulk conductivity to the total ionic conductivity.

Acknowledgements

The financial support by the Ministry of Education and Science of the Republic of Kazakhstan by grant funding project AP05135273 and AP06851299 by the Ministry of Industry and Infrastructural Development of the Republic of Kazakhstan are gratefully acknowledged.

References

[1]. F. Yu, T. Han, Z. Wang, Y. Xie, Y. Wu, Y. Jin, N. Yang, J. Xiao, S. Kawi, *Int. J. Hydrogen Energ*. 46 (2021) 4283–4300. DOI: 10.1016/j.ijhydene.2020.10.259

[2]. L. Li, J. Lin, N. Wu, S. Xie, C. Meng, Y. Zheng, X. Wang, Y. Zhao, *Energy and Built Environment* (*In Press*), 2020. DOI: 10.1016/j.enbenv.2020.12.002

[3]. F.R. Sultanov, C. Daulbayev, B. Bakbolat, Z.A. Mansurov, *Eurasian Chem.-Technol. J*. 20 (2018) 195–200. DOI: 10.18321/ectj721

[4]. F.R. Sultanov, Ch. Daulbayev, B. Bakbolat, Z.A. Mansurov, A.A. Urazgaliyeva, Rabi Ebrahim, S.S. Pei, Kun-Ping Huang, *Carbon Lett*. 30 (2020) 81–92. DOI: 10.1007/s42823-019-00073-5

[5]. B. Yang, Z. Guo, J. Wang, J. Wang, T. Zhu, H. Shu, G. Qiu, J. Chen, J. Zhang, *J. Energy Storage* 34 (2021) 102153. DOI: 10.1016/j.est.2020.102153

[6]. Z. Zeng, Y. Qian, Y. Zhang, C. Hao, D. Dan, W. Zhuge, *Appl. Energ*. 280 (2020) 115899. DOI: 10.1016/j.apenergy.2020.115899

[7]. M. Ma, X. Yang, J. Qiao, W. Sun, Z. Wang, K. Sun, *J. Energy Chem.* 56 (2021) 209–222. DOI: 10.1016/j.jechem.2020.08.013

[8]. A.J. Abd Aziz, N.A. Baharuddin, M.R. Somalu, A. Muchtar, *Ceram. Int*. 46 (2020) 23314–23325. DOI: 10.1016/j.ceramint.2020.06.176

[9]. D. Ding, X. Li, S. Yuxiu Lai, K. Gerdes, M. Liu, *Energ. Environ. Sci.* 7 (2014) 552–575. DOI: 10.1039/c3ee42926a

[10]. M.J. Glenn, J.A. Allen, S.W. Donne, *J. Power Sources* 453 (2020) 227662. DOI: 10.1016/j.jpowsour.2019.227662

[11]. M. Benamira, A. Ringuedé, V. Albin, R.-N. Vannier, L. Hildebrandt, C. Lagergren, M. Cassir, *J. Power Sources* 196 (2011) 5546–5554. DOI: 10.1016/j.jpowsour.2011.02.004

[12]. J. Hou, M. Yang, J. Zhang, *Renew. Energ*. 155 (2020) 1355–1371. DOI: 10.1016/j.renene.2020.04.002

[13]. Y. Prykhodko, K. Fatyeyeva, L. Hespel, S. Marais, *Chem. Eng. J*. 409 (2021) 127329. DOI: 10.1016/j.cej.2020.127329

[14]. X. Xu, Y. Xu, J. Ma, Y. Yin, M. Fronzi, X. Wang, L. Bi, *J. Power Sources* 489 (2021) 229486. DOI: 10.1016/j.jpowsour.2021.229486

[15]. F.R. Sultanov, B. Bakbolat, Z.A. Mansurov, *Eurasian Chem.-Technol. J*. 19 (2017) 127–132. DOI: 10.18321/ectj286

[16]. R.E. Beissenov, A.L. Mereke, A.G. Umirzakov, Z.A. Mansurov, B.A. Rakhmetov, Y.Y. Beisenova, A.A. Shaikenova, D.A. Muratov, *Mat. Sci. Semicon. Proc.* 121 (2021) 105360. DOI: 10.1016/j.mssp.2020.105360

[17]. C.B. Daulbaev, T.P. Dmitriev, F.R. Sultanov, Z.A. Mansurov, E.T. Aliev, *J. Eng. Phys. Thermophys*. 90 (2017) 1115–1118. DOI: 10.1007/s10891-017-1665-z

[18]. M. Agarwal, V. Kumar, S.R.K. Malladi, R. Balasubramaniam, K. Balani, *JOM* 62 (2010) 88–92. DOI: 10.1007/s11837-010-0095-6

[19]. X. Lv, H. Chen, W. Zhou, F. Cheng, S.-D. Li, Z. Shao, *Renew. Energ.* 150 (2020) 334–341. DOI: 10.1016/j.renene.2019.12.126

[20]. J.W. Fergus, *Solid State Ionics* 177 (2006) 1529–1541. DOI: 10.1016/j.ssi.2006.07.012

[21]. R. Ebrahim, M. Yeleuov, A. Ignatiev, *Adv. Mater. Technol.* 2 (2017) 1700098. DOI: 10.1002/admt.201700098

[22]. Z. Zakaria, S.H. Abu Hassan, N. Shaari, A.Z. Yahaya, Y. Boon Kar, *Int. J. Energ. Res.* 44 (2019) 631–650. DOI: 10.1002/er.4944

[23]. H. Hidalgo, E. Reguzina, E. Millon, A.-L. Thomann, J. Mathias, C. Boulmer-Leborgne, T. Sauvage, P. Brault, *Surf. Coat. Tech*. 205 (2011) 4495–4499. DOI: 10.1016/j.surfcoat.2011.03.077

[24]. A. Nenning, M. Gerstl, M. Bram, A.K. Opitz, *ECS Trans*. 91 (2019) 479–490. DOI: 10.1149/09101.0479ecst

[25]. A. Hauch, M. Mogensen, *Solid State Ionics* 181 (2010) 745–753. DOI: 10.1016/j.ssi.2010.04.001

[26]. A. Buyukaksoy, V. Birss, *ECS Trans*. 66 (2015) 253–265. DOI: 10.1149/06602.0253ecst

[27]. Sam Zhang, Organic Nanostructured Thin Film Devices and Coatings for Clean Energy, Chapter 5: Thin Coating Technologies and Applications in High-Temperature Solid Oxide Fuel Cells, 1st Edition, 2010, CRC Press. DOI: 10.1201/b11846

[28]. P. Holtappels, C. Sorof, M.C. Verbraeken, S. Rambert, U. Vogt, *Fuel Cells* 6 (2006) 113–116. DOI: 10.1002/fuce.200500116

[29]. J.J. Haslam, A.-Q. Pham, B.W. Chung, J.F. DiCarlo, R.S. Glass, *J. Am. Ceram. Soc.* 88 (2005) 513–518. DOI: 10.1111/j.1551-2916.2005.00097.x

[30]. K.S. Walton, R.Q. Snurr, *J. Am. Chem. Soc*. 129 (2007) 8552–8556. DOI: 10.1021/ja071174k

[31]. C. Suciu, E. Dorolti, A.C. Hoffmann, *Mater. Sci. Energy Technol.* 1 (2018) 136–145. DOI: 10.1016/j.mset.2018.06.007